Mechanical behavior of entangled materials with or without cross-linked fibers

J.-P. Masse[a,*] and D. Poquillon[b]

[a] *Arcelor Mittal Research, Voie Romaine, BP30320, 57283 Maizières-lès-Metz Cedex, France*
[b] *Université de Toulouse, CIRIMAT, INP-ENSIACET, 4 allée Emile Monso, BP 44362, 31030 Toulouse Cedex 4, France*

Abstract—Entangled materials can be manufactured using fibers made from various materials, such as carbon, glass or steel. The mechanical properties of these low-density materials are linked to their architecture (fiber orientation, number of contacts, etc.). Specimens can be produced with and without cross-links between fibers by sintering for steel wool or by using epoxy spraying for carbon or glass fibers. Experimental mechanical compression tests were performed on these materials. The results were analyzed taking into account the architecture thanks to the relationships existing between morphological data and macroscopic mechanical behavior.

Keywords: Entangled materials; Carbon/glass fibers; Metallic fibers; Mechanical behavior; 3-D tomography

1. Introduction

Entangled materials are composed of fibers which can be made from natural materials (e.g. wool or cotton) or artificial materials (e.g. carbon fibers, glass fibers or steel fibers). These materials are used for thermal insulation, mechanical reinforcement and filtration. Considering their low relative density and their internal architecture, they can be considered similar to cellular materials. Their properties depend on their architectural parameters, which are the number of contact points, the orientation of the fibers and their dimensions (aspect ratio). The nature of the contacts is also a parameter which influences the properties of entangled materials; indeed, it is possible to create permanent and non-permanent contacts. Processes to make entangled materials can be simple, and their use has recently been studied as a core material for sandwich structures [1–5]. Indeed, they present an alternative to foams (metal or polymer), the use of which can be limited due to weldability issues or the addition of functions. For some metals, e.g. steel, foams are difficult to process because of the high melting point, and the use of steel fibers is simpler. This is why many studies have been performed on these materials, testing their mechanical properties (compression, tension, bending), thermal and electrical conductivity, and also damping properties [4–12]. To predict the properties of materials made of entangled fibers, analytical and numerical modeling has been developed. In compression, a simple analytical model shows that the stress follows a power law of the relative density, assuming that the fiber bends during compression [13]. Numerical simulation can be achieved by finite element methods [14] and molecular dynamic simulations [15], and confirms that point. Analytical approaches are in general based on models describing the number of contacts as a function of the relative density and the fiber orientation distribution for non-permanent contacts. That is why studies on entangled materials focus on structural characterization to assess these parameters.

The aim of this work is to show a compilation of different studies on various entangled materials (carbon fibers, glass fibers, steel fibers) with or without permanent cross-links between fibers. It focuses on differences in mechanical behavior in compression with or without permanent cross links, followed by structural characterization and comparison with the models found in the literature.

2. Example of entangled materials

Various entangled materials were analyzed and are presented in Figure 1. Glass fibers (Fig. 1a) and carbon fibers (Fig. 1b) with a circular cross-section were obtained from yarn. Their diameters were 12 and 7 μm, respec-

* Corresponding author; e-mail: jean-philippe.masse@arcelormittal.com

http://dx.doi.org/10.1016/j.scriptamat.2012.05.047

Table 1. Experimental values of n for glass, carbon and steel fibers in entangled materials without permanent contacts.

Materials	ρ_0 (%)	n
Glass fibers	5.7	2.50
	8.5	2.74
	11.4	2.87
Carbon fibers	4	2.81
	5.9	3.17
	7.9	3.07
Steel wool	1.5	3.22
	2.2	3.91
	3.2	4.15

tively, their Young's moduli were 73 and 240 GPa, and their length was 40 mm. For both materials, epoxy resin was used to cross-link the fibers. Approximately 30 nm of resin was coated onto the fibers by spraying. Typical structures after polymerization are presented in Figure 1a and b. Stainless steel wool (Fig. 1c) was also tested. Its dimensions and shape were neither constant nor homogeneous, but its mean equivalent diameter was 80 μm and its mean length was 5.6 cm. In order to create permanent cross-links in the structure, sintering at temperatures between 1300 and 1400 °C was performed for durations of between 1 and 5 h. Figure 1d shows a contact obtained after sintering at 1300 °C for 1 h. With this method, it was observed that not all the cross-links were sintered. The ranges of relative density of glass fibers, carbon fibers, steel wool and partially sintered steel wool were respectively 6–11%, 5.5–12%, 1.6–5.4% and 4–12%.

3. Mechanical characterization

Quasi-static compression tests were performed on each material. For glass and carbon fibers without permanent cross-linking, confined compression was applied; for steel wool, and glass and carbon fibers with permanent cross-links, simple compression is applied.

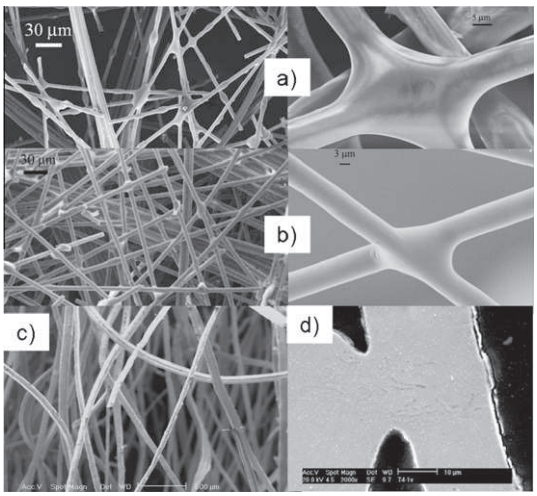

Figure 1. Pictures of entangled materials images with or without permanent cross link (a) glass fiber, $\rho_0 = 5.9\%$, with epoxy cross link (b) carbon fibers $\rho_0 = 8.5\%$ (c) steel wool $\rho_0 = 1.8\%$ (d) sintered steel wool $\rho_0 = 5\%$.

Stress (σ) and strain (ε) were calculated from measurements of the displacement and the force following the equations:

$$\sigma = \frac{F}{S} \quad \varepsilon = \ln\left(\frac{h}{h_0}\right) \quad \text{and} \quad \rho = \rho_o \exp(-\varepsilon) \tag{1}$$

where S is the sample section, h is the length of the sample and h_0 is the initial length of the sample. Considering that S is unchanged during compression, the relative density (ρ) is given as a function of the initial relative density ρ_0 and the strain.

Figure 2a shows the stress–strain curves for materials made from entangled carbon fibers with and without permanent cross-linking, whereas in Figure 2b stress as a function of relative density is presented on a log–log scale for non-sintered steel wool. These two representations can be used for entangled materials if the section of the sample does not change during the compression test.

Two kinds of behavior were identified from these results. Materials with permanent cross-links exhibited a behavior which can be divided into three steps. The first is the elasticity of the network; new contacts can be ignored. The second step corresponds to an increasing plateau, with both creation of new friction contacts between fibers and the fracture of some cross-links. The last step corresponds to a densification, and most of the initial cross-links are broken. The compression behavior is thus comparable to that of the material without cross-links.

In the case of non-permanent cross-links, only the third step is observed: the entangled material has low initial stiffness, and new contacts are created from the start of the compression with increasing density. The stress–relative density curve can be fitted by a power law which corresponds to Toll's model, which will be explained later in the paper.

The presence of permanent cross-linking between fibers greatly stiffens the material in steps one and two. The Young's moduli for the entangled fibers without epoxy cross-links are far lower than that of the same material with epoxy cross-links: for entangled carbon fibers (8.5% volume fraction), a value of 0.9 instead of 7.5 MPa, and for entangled glass fibers (6% volume fraction), a value of 0.3 instead of 1.7 MPa. However, scanning electron microscopy (SEM) observations of interrupted tests show that not all junctions are broken in step two. Their persistence limits the reorganization of the fibers contrary to the case of entangled fiber without epoxy cross-links.

As X-ray microtomography does not allow us to separate glued contacts from contacts with friction, only SEM observations after interrupted compression tests can help us to get a better understanding of the mechanisms. For the entangled fibers without epoxy cross-links, increasing the compression decreases the number of fibers oriented in the direction of the load. Broken fibers are very rare, even after large (60%) compression. Observations thus tend to show that, under compression, fibers rearrange without being broken, and the entanglement becomes denser and increases its rigidity. For the entangled fibers with epoxy cross-links, broken junctions and fibers are observed during stages 2 and

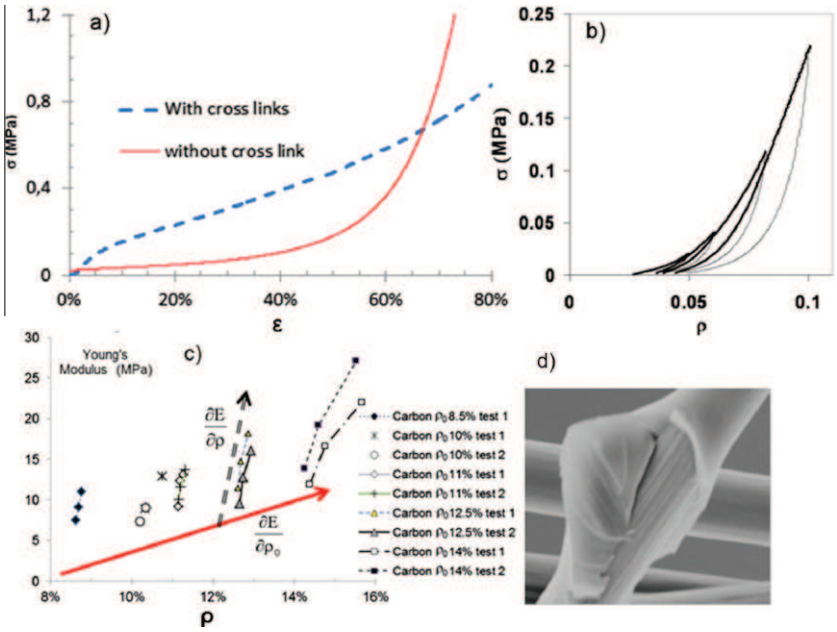

Figure 2. Compression stress on (a) carbon fiber ($\rho_0 = 8.5\%$) with and without epoxy cross link represented as a function of compression strain (b) non sintered steel wool ($\rho_0 = 3\%$) represented as a function of relative density, 4 unload are performed (c) Young's Moduli measured during compression tests on entangled materials made with cross-linked carbon fibers. Samples with 5 different initial fiber volume fractions ρ_0 were tested. For each sample, Young's Modulus was measured at different strains so for an increasing density of the materials (d) broken epoxy cross-links on carbon fiber ($\rho_0 = 8.5\%$) with epoxy cross link after a 40% compression.

3, and fiber reorientation occurs. However, the rigidity of the fiber network whose density is increasing is offset by the increasing flexibility due to junctions and broken fibers (Fig. 2d). This might explain why the curves intersect in Figure 2a. However, only X-ray tomography carried out on a representative volume element with a sufficient resolution can provide statistical quantitative data.

Specific tests were conducted to better understand, for materials with epoxy junctions, the stiffness due to non-cross-linked contacts (typically, newly formed contacts, which become increasingly abundant during compression) and the stiffness from the epoxy junctions.

Young's moduli were measured during compression tests by successive discharges between 1% and 3% deformation for entangled cross-linked materials with a fiber volume fraction between 8.5% and 14%. Results are illustrated in Figure 2c for carbon fibers and the same evolution was obtained for aramid and glass fibers. For a given test which corresponds to a known initial fiber ρ_0 volume fraction, the Young's modulus E increases during compression: $E = E(\rho_0,\varepsilon) = E(\rho_0, \rho - \rho_0)$. This corresponds to the activation of new contacts. For a sample made with a larger fiber volume fraction f_1, the Young's modulus is larger for a given strain $E(\rho_0, \varepsilon_0) < E(\rho_1, \varepsilon_0)$, which seems to results from a larger number of cross-linked contacts (SEM observations). The modulus increases faster with compression ε than the initial fiber volume fraction ρ_0: $\frac{\partial E(\rho_0,\varepsilon)}{\partial \rho_0} = \frac{\partial E(\rho_0,\rho)}{\partial \rho_0} >> \frac{\partial E(\rho_0,\rho)}{\partial \rho}$. This effect of densification does not seem to depend on ρ_0 in the tested range. On the other hand, we have no statistics to measure the increase of the number of junctions per unit volume or the decrease in average length between contacts vs. ρ_0 evolution.

4. Models

To predict mechanical properties in compression, two kinds of model were developed, corresponding to the different steps identified in the compression curves. To predict elasticity, Markaki and Clyne proposed [11] an expression for the elastic modulus E:

$$E = \frac{9E_f\rho}{32(\lambda/d_f)^2} \tag{2}$$

With d_f the diameter of the fibers, λ the length between contacts, E_f the Young's modulus of the fibers and ρ the relative density.

For densification, Toll extended Van Wyk's work and proposed a relation between the stress in compression and the relative density [13]:

$$\sigma = kE_f(\rho^n - \rho_0^n) \tag{3}$$

Again, E_f is the Young's modulus of the fibers, and k is a multiplicative factor depending on the loading direction of the fibers. The exponent n depends on the orientation; its value is 3 for random 3-D orientation and 5 for random 2-D orientation. The assumptions of this model are that fibers work in bending, the aspect ratio of the fibers is high and the orientation of the fibers does not change during compression. It is based on the "tube model" for the number of contacts. For example, for a high aspect ratio the number of contact per unit of volume is:

$$N_{cv} = \frac{16f}{\pi^2 d_f^3}\rho^2 \text{ with } f = \frac{1}{N_f^2}\sum_{\alpha}\sum_{\beta}\|p_\alpha \times p_\beta\| \tag{4}$$

where f is an orientation function calculated from the director vector of a fiber (p_α and p_β, with α and β

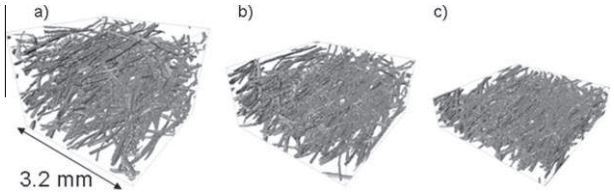

Figure 3. 3D visualization of a non sintered steel wool with an initial relative density of 2% during in situ compression test at different relative densities: (a) 3.8% (b) 5.3% (c) 9%.

defining fibers). This function is assumed to be constant in Toll's model. In Ref. [16], n values were identified ranging from 2.5 to 3.9 for entangled glass or carbon fibers. Increasing the initial density of the material increased the value of n due to the fabrication process as the random entanglement of fibers must be placed in a mold. The closing of the lid to reach the desired fraction changes the orientation of fibers (from 3-D to 2-D). In Ref. [1] measurements show that n ranges from 3.2 to 4.15 for tested non-sintered steel wools. The value of n for these different materials is summarized in Table 1.

5. Structural characterization

The different analytical models introduced in the previous paragraphs take into account the following elements in their expression:

- fiber orientation distribution
- number of contacts
- length between contacts

These data must be known to explain and predict the behavior of entangled materials. In materials with permanent cross-links, the length between contacts seems to be the critical parameter. One way to measure it is to observe it using SEM, but getting relevant statistical information on the average distance between contacts and on fiber orientation using this technique is time consuming. A more efficient technique is to use X-ray tomography. It is possible to compute all these data from the 3-D images. This was done for steel wool [1]. One method involves obtaining the skeleton (Fig. 3) of the structure from the 3-D volume. In shape analysis, the skeleton (or topological skeleton) of a shape is a thin version of that shape that is equidistant from its boundaries. From the skeleton obtained from Ref. [17], it is possible to detect the contacts and extract the coordinates of each line between them, and then compute the orientation of the fibers [1].

From these measurements, it is possible to check the assumptions of Toll's model: fiber orientation was found to be constant during loading, and the number of contacts followed a power law relating the relative density with an exponent of 2. Figure 4 shows the number of contacts and fiber orientation (function f) extracted from in situ compression in X-ray tomography of a non-sintered steel wool with an initial relative density of 3.2%. These results show that the orientation is not constant during compression (Fig. 4b), as assumed in Toll's model. Moreover, the number of contacts per unit volume did not follow the square of the relative density. The value of f also shows that fiber orientation does not differ between two dimensions ($f = 2/\pi$) and three dimensions ($f = \pi/4$) in this case. The value of n was explained taking this into account in Ref. [2].

6. Discussion

Obtaining a representative volume element during X-ray tomography does not provide sufficient accuracy to determine whether a contact is sintered or bonded or not. Thus, no statistical data are available to quantify the density of bonded contacts or the density of friction contacts. These points are as important as the fiber orientation distribution in modeling the mechanical and electrical properties of these entangled cross-linked materials.

However, X-ray tomography does provide data on the modifications to fiber orientation that occur during mechanical testing. These data can be used directly for non-cross-linked materials using a Toll model [13]. However, this approach is not suitable for describing the hysteresis observed during unloading or the viscoelastic effects [18]. Modeling friction between fibers is the key point in this case [19], and an approach taking

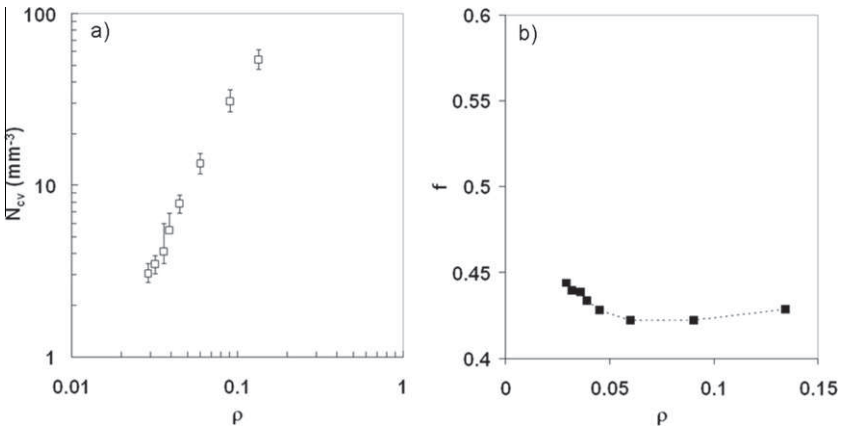

Figure 4. Evolution of the number contact per unit volume (N_{cv}) and the orientation function f as a function of the relative density during a compression test on a non sintered steel wool of initial relative density of 3.2% from X-ray tomography in situ test.

into account the number of contacts before unloading and the number of contacts destroyed during unloading allows the first step of unloading to be described.

However, no model is yet available to predict the initial network elasticity, the stress level for which begins in step two, the associated slope or, finally, the behavior during the third stage (consolidation).

7. Conclusion

In this paper, we have studied a variety of entangled materials, such as glass, carbon and steel fibers entangled with or without permanent cross-linking between the fibers. From the analysis, several points have emerged:

- The mechanical behavior of entangled materials can be tailored by controlling the density of contacts and permanent contact between fibers. Materials produced with no permanent contacts show completely different behavior from those with a high density of permanent contacts. In the first case, the material has a very low rigidity, which increases during compression due to the increasing number of contacts created. In the second case, the initial rigidity is higher than that of the materials with no permanent contacts. During compression, the breaking of permanent contacts induces a reduction in stress compared with the case with no permanent contacts. The choice of whether to add permanent contacts or not will depend on the desired rigidity and the compression strain that will be imposed on the materials.
- Models exist to predict the elasticity (for permanent contacts) and densification (for non-permanent contacts) of the materials, but work has to be done to extend these models taking into account the nature of the contacts and the fiber orientation for the elastic model.
- X-ray tomography coupled with skeleton plotting is a powerful tool for studying the architectural parameters of entangled materials in order to link the architecture to properties via analytical models. Currently, one of the weaknesses of this tool is that it is very difficult to differentiate permanent and non-permanent contacts.

References

[1] J.P. Masse, 2009, PhD Thesis, Grenoble INP.
[2] L. Mezeix, 2010 PhD Thesis, Universtité de Toulouse.
[3] J.P. Masse, Y. Bréchet, L. Salvo, O. Bouaziz, in: Y.Bréchet, J.D. Embury, P.R. Onck (eds.), Architectured Multifunctional Materials, Materials Research Society Symposium Proceedings Vol. 1188, paper 5, Cambridge University press, 2009.
[4] A.E. Markaki, T.W. Clyne, Acta Mater. 51 (5) (2003) 1341–1350.
[5] A.E. Markaki, T.W. Clyne, Acta Mater. 51 (5) (2003) 1351–1375.
[6] A. Shahdin, J. Morlier, Y. Gourinat, L. Mezeix, C. Bouvet, J. Sandwich Struct. Mater. 12 (5) (2010) 569–589.
[7] I.O. Golosnoy, A. Cockburn, T.W. Clyne, Adv. Eng. Mater. 10 (3) (2008) 210–218.
[8] B.M. Zhang, S.Y. Zhao, X.D. He, J. Quant. Spectrosc. Ra. 109 (7) (2008) 1309–1324.
[9] J. Dean, P.M. Brown, T.W. Clyne, In: Ferreira (Ed.), Proceedings of the 8th International Conference on Sandwich Structure (ICCS8), Portugal, 2008, p. 199.
[10] J.P. Masse, K. Beyer, D. Bouvard, O. Bouaziz, Y. Bréchet, Adv. Mater. Research 47–50 (2008) 121–124.
[11] A.E. Markaki, T.W. Clyne, Acta Mater. 53 (2005) 877–889.
[12] R. Gustavsson, Patent WO 98/01295, AB Volvo, 15 January 1998.
[13] S. Toll, Polym. Eng. Sci. 38 (1998) 1337–1350.
[14] D. Durville, J. Mater. Sci. 40 (22) (2005) 5941–5949.
[15] C. Barbier, R. Dendievel, D. Rodney, Comp. Mater. Sci. 45 (3) (2009) 593–596.
[16] L. Mezeix, C. Bouvet, J. Huez, D. Poquillon, J. Mater. Sci. 44 (14) (2009) 3652–3661.
[17] Avizo 5: http://www.scientificcomputing.com/Avizo-5.aspx.
[18] D. Poquillon, B. Viguier, E. Andrieu, J. Mater. Sci. 40 (22) (2005) 5963–5970.
[19] C. Barbier, R. Dendievel, D. Rodney, Phys. Rev. E 80 (2009) 016115–016120.